International Journal of Machine Tools & Manufacture 48 (2008) 1072–1080

Contents lists available at ScienceDirect

International Journal of Machine Tools & Manufacture

journal homepage: www.elsevier.com/locate/ijmactool

Modelling tool wear in cemented-carbide machining alloy 718

J. Lorentzon *, N. Järvstråt

Department of Technology, University West, Gustava Melins gata 2, Trollhättan, Sweden

ARTICLE INFO

Article history:
Received 3 January 2008
Received in revised form
28 February 2008
Accepted 2 March 2008
Available online 18 March 2008

Keywords:
Tool wear
FEM
Inconel 718
Friction
Modelling

ABSTRACT

Tool wear is a problem in turning of nickel-based superalloys, and it is thus of great importance to understand and quantitatively predict tool wear and tool life. In this paper, an empirical tool wear model has been implemented in a commercial finite element (FE) code to predict tool wear. The tool geometry is incrementally updated in the FE chip formation simulation in order to capture the continuous evolution of wear profile as pressure, temperature and relative velocities adapt to the change in geometry. Different friction and wear models have been analysed, as well as their impact on the predicted wear profile assessed. Analyses have shown that a more advanced friction model than Coulomb friction is necessary in order to get accurate wear predictions, by drastically improving the accuracy in predicting velocity, thus having a dramatic impact on the simulated wear profile. Excellent experimental agreement was achieved in wear simulation of cemented carbide tool machining alloy 718.

1. Introduction

Nickel-based superalloys, used in the aerospace industry, are among the most difficult materials to machine. These alloys are designed to retain their high strength at elevated temperatures, and machining thus involves forces that are considerably higher than those found in the machining of steel. In addition, the contact length is shorter, which gives rise to high stresses at the tool–chip interface [1]. Work hardening, which can be as much as 30 percent [2], is another problem encountered when machining these alloys, as it may lead to severe tool wear at the flank face. The low thermal conductivity of nickel alloys giving rise to high temperature is yet another problem [3], and temperature measurements [1] have shown that the temperature is higher than for steel.

The high stress at the tool–chip interface, the work hardening, and the high temperature involved in the machining of nickel alloys all contribute to tool wear. It is therefore important to understand the wear process in order to predict wear rates and improve tool life. In the past, experimentation has been the main method used for investigating wear. However, continuous development of numerical methods such as the finite element method (FEM) together with more powerful computers enables simulation of complicated contact problems such as the cutting processes.

FEM has proved to be an effective technique for analysing the chip formation process and predicting process variables such as temperatures, forces, stresses, etc. Therefore, the use of simulations has increased considerably over the past decade, and coupled thermo-mechanical simulation of the chip formation process has been used by many researchers, such as MacGinley and Monaghan [4], Yen et al. [5], Altan et al. [6], Hortig and Svendsen [7]. Lately, simulations of the evolution of tool wear have also been performed by implementing a wear rate equation, such as Usui's equation, in FE software. The method has been used by Yen et al., Filice et al., and Xie et al. [8–10] for steel, calculating the wear rate from predicted cutting variables, and updating the geometry by moving the nodes of the tool. Reasonably good accuracy was achieved, and the method can be regarded as state-of-the-art in modelling of machining.

However, this approach for simulation of tool wear in machining nickel-based superalloys has shown considerable discrepancy between simulated and measured geometry, especially in the region around the tool tip [11]. Consequently, more work is required to enable accurate tool wear simulations. To do this properly, it is necessary to simultaneously work with modelling wear and friction at the tool–chip interface, as these phenomena are strongly related. According to Amonoton's law the frictional stress is proportional to normal stress. However, Childs [12] states that frictional stress is limited when the normal stress is larger than the shear flow stress. This is the case in the region around the tool tip, where the real-contact area approaches the nominal contact area [12]. Özel [13] evaluated different friction models and suggests that "variable friction models should be used in order to obtain more accurate results in FE simulations of

* Corresponding author. Tel.: +46 706 51 34 47; fax: +46 520 22 30 99.
E-mail addresses: john.lorentzon@hv.se, john.jl.lorentzon@volvo.com (J. Lorentzon).

0890-6955/$ - see front matter © 2008 Elsevier Ltd. All rights reserved.
doi:10.1016/j.ijmachtools.2008.03.001

machining''. This has not been considered in previous tool wear simulations, where the friction has been described with constant friction coefficient over the tool–chip interface by the shear model [8,9], or by Coulomb friction [10,11].

1.1. Objective

The overall objective of this work is to develop a finite element tool wear model that can predict the worn geometry quantitatively in cemented carbide tool machining nickel-based alloys. To achieve this, different wear and friction models' impact on parameters affecting the wear process, such as temperature and relative velocity, have been investigated and used for predicting the worn tool geometry. Specifically, the details analysed here are divided into wear and friction (described in more detail in Sections 2.1.4 and 2.2):

1.1.1. Wear

W1. Usui's empirical wear rate model [14–16], which is a function of contact pressure, relative velocity and absolute temperature;
W2. For Usui's model, a second set of parameters giving a different temperature dependency is also investigated;
W3. Takayama and Murata's [17] wear rate model, including a functional dependence of absolute temperature;
W4. Modified Usui wear rate model, by adding an exponent on the relative velocity;
W5. Vibration-adjusted Usui model, where a constant term is added to the relative velocity to account for vibrations, which are not included in the chip formation model.

1.1.2. Friction

F1. Coulomb friction model, which states that the friction force is proportional to the contact pressure;
F2. Shear friction model, which states that the friction force is a fraction of the equivalent stress;
F3. Coulomb friction model with two different friction coefficients, a reduced one around the tool tip and at a distance up on the rake face.

2. Tool wear model

The tool wear model consists of a FE chip formation model and a wear model implemented as subroutines to calculate the wear rate at contact points, modifying the tool geometry accordingly.

2.1. Chip formation model

The FE chip formation model was created using the commercial software MSC. Marc, which uses an updated Lagrange formulation. This means that the material is attached to the mesh, with periodic remeshing to avoid element distortion. The cutting process requires a coupled thermo-mechanical analysis, because mechanical work is converted into heat, causing thermal strains and influencing the material properties. Two types of thermal assumptions are commonly used for simulation of mechanical cutting, namely adiabatic heating and fully coupled thermal–mechanical calculations. In this work a coupled, staggered, model has been used. This means that for each time increment the heat transfer analysis is made first, followed by the stress analysis. The time increment was set to 1.5 μs in all analyses. Quasi-static analyses were used, which means that the heat analysis is transient, while the mechanical analysis is static with inertial forces neglected.

2.1.1. Dimensions

The dimensions of the workpiece used in the simulation model are 5 mm length by 0.5 mm height, and the tool used in the simulation model is 2 mm long and 2 mm high, see Fig. 1. The cutting-edge radius was set to 16 μm in agreement with measurement (see Fig. 1), the clearance angle 6° and the rake angle 0°; the feed was 0.1 mm and the cutting speed was 0.75 m/s.

2.1.2. Mesh

The meshed workpiece can be seen in Fig. 1. The remeshing technique used was the ''advancing front quad''. This mesh generator starts by creating elements along the boundary of the given outline boundary and mesh creation continues inward until the entire region has been meshed. The number of elements used was about 6000, with the minimum element size set at 2 μm. As seen in Fig. 2a, finer mesh was used where the material separates around the tool tip. The tool was meshed with approximately 5000 elements, with minimum element size being 2 μm.

2.1.3. Material properties

Generally, the strain magnitude, the strain rate, and the temperature each have a strong influence on the material flow stress. Thus, it is necessary to capture these dependencies in the material model used, in order to correctly predict the chip formation. Here, neglecting a slight (about 10% between 1/s and

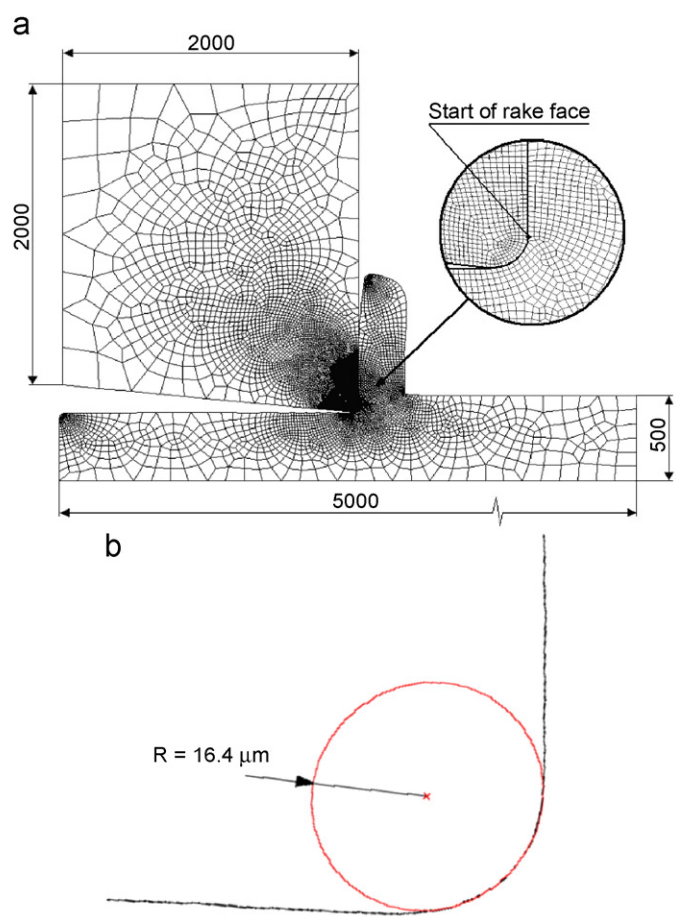

Fig. 1. (a) Dimension of the chip formation model, scaled in μm. The start of the rake face is marked, as it will serve as a reference point in the wear profiles. (b) The measured cutting-edge shape, with the radius indicated; the measurement method is presented in Section 4.2.

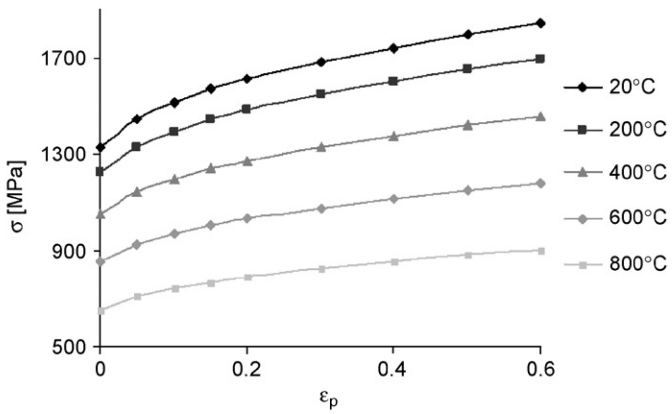

Fig. 2. Flow stress curves (curve at room temp from [18] and thermal softening from [20]).

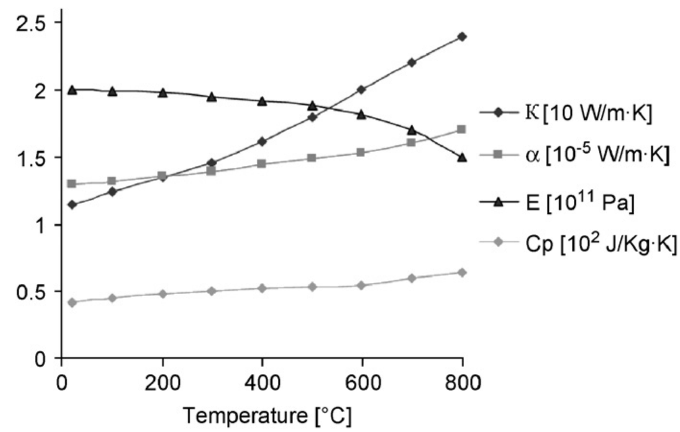

Fig. 3. Young's modulus, E, specific heat, C_p, thermal conductivity, K, and thermal expansion, α, from [21].

10^4/s at room temperature according to [18] and nearly zero between 10^2/s and 10^5/s at 300 °C according to [19]) strain rate dependency, a rate-independent piecewise linear plasticity model was used. Instead, the flow stress curve after [18] for high strain rate (10^4/s) was used, see Fig. 2. The temperature trend of the flow stress is taken from [20]. The other work-piece material properties [21] used can be seen in Fig. 3.

The material properties of the uncoated cemented carbide tool were considered independent of temperature, and are listed in Table 1.

Table 1
Tool material properties for the cemented carbides [4,5,22]

Density (Kg/m^3)	11,900 [4]
Young's modulus (GPa)	630 [22]
Poisson's ratio	0.26 [5]
Yield limit (MPa)	4250 [22]
Thermal expansion	5.4×10^{-6} [5]
Specific heat (J/Kg K)	334 [4]
Thermal conductivity (W/m K)	100 [22]

2.1.4. *Friction at the tool–chip interface*

In this work, three different friction descriptions have been used. In each case the friction coefficient was calibrated to correlate within 5% on the simulated and measured feed force. The feed force is the sum of the ploughing force and the friction force. However, in our case the cutting edge radius is small compared to the feed rate (see Fig. 1), limiting the ploughing effect, and consequently friction provides a considerable part of the feed force. The models used are:

F1: The Coulomb friction model states that the friction force is proportional to the contact pressure through a friction coefficient, μ, Eq. (1). The friction coefficient, μ, was set to 1.0:

$$\sigma_t = -\mu\sigma_n \tag{1}$$

F2: A shear friction model, which states that the friction force is a fraction of the equivalent stress, Eq. (2). The friction coefficient, m, was set to 1.1:

$$\sigma_{fr} = m\frac{\sigma_{eqv}}{\sqrt{3}} \tag{2}$$

F3: The Coulomb friction model as for F1, but here with two different friction coefficients, μ, over the tool–chip interface. Around the tool tip and at a distance up on the rake face, where the contact pressure is extremely high (above 1000 MPa), the friction coefficient is set to 0.75. Elsewhere the friction coefficient is set to 1.1. A principle sketch of this is seen in Fig. 4. The model is a simplified representation of the physical behaviour observed by Zorev [23], that there is a cap on the friction stress at high normal stress.

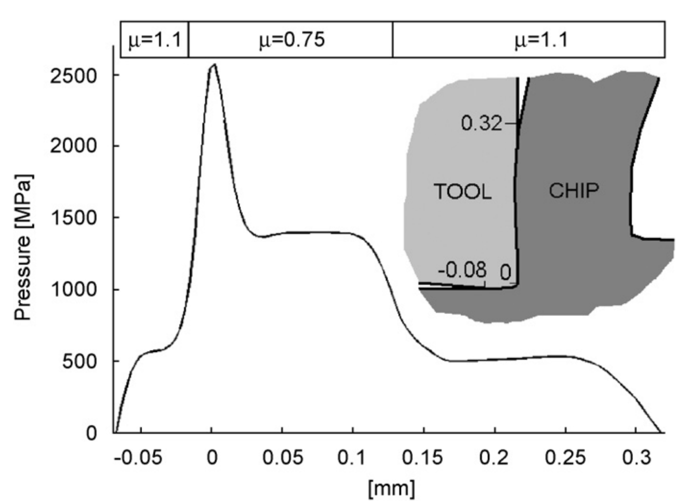

Fig. 4. Pressure along tool–chip interface, with regions for the different friction coefficients marked.

2.1.5. *Heat generation*

In the machining process heat is generated by friction and plastic deformation. The rate of specific volumetric flux due to plastic work is given by

$$\dot{q} = \frac{f\dot{W}_p}{\rho} \tag{3}$$

Here, $\dot{W}_p$ is the rate of plastic work, ρ is the density and f is the fraction of plastic work converted into heat, which is set to 1. Strictly speaking, this is not correct since some plastic work is stored in the material, but the relative fraction stored is unknown, and since the deformations are so large the fraction of plastic work stored is neglected. The rate of heat generated due to friction is given by

$$\dot{Q} = F_{fr}v_r \tag{4}$$

Here, F_{fr} is the friction force and v_r is the relative sliding velocity. The heat generated due to friction is equally distributed

Table 2
Wear model parameters for friction model F1

W1	W2	W3	W4	W5
$A = 1.25 \times 10^{-12}$ $B = 8900$	$A = 5.48 \times 10^{-15}$ $B = 2000$	$D = 1.02 \times 10^{-9}$ $E = 75350$	$A' = 5.42 \times 10^{-13}$ $B = 8900$	$A'' = 1.08 \times 10^{-15}$ $B = 8900$

into the two contact bodies. This heat is transferred from the workpiece, due to convection to the environment and conduction to the tool. Radiation has been neglected. The heat transfer coefficient at the contact between the tool and the workpiece was set to 1000 kW/m^2 K, which according to Filice et al. [24] permits a satisfactory agreement between numerical data and the experimental evidence, although it should be noted that this was utilised for another material combination. The temperature at the outer boundaries of the tool was fixed at room temperature.

2.2. Wear model

There are few wear rate models for cutting available in literature. Two of the more important have been used in this work, and a further two modified versions of one have been tested:

W1: Usui's [14–16] empirical wear rate model Eq. (5) models the wear rate as a function of contact pressure, o'_n, relative velocity, v_{rel} and absolute temperature, T:

$$\frac{dw}{dt} = A\sigma_n v_{rel} e^{-B/T} \tag{5}$$

W2: A different parameter set was also tested in order to investigate the impact of the temperature dependency.

W3: Takeyama and Murata's [17] wear rate model Eq. (6) is able to account for diffusion wear dominating at higher temperature. The model is a function of the absolute temperature, T, and the constants are D, which is a material constant, E, the activation energy and R (8.314 kJ/mol K), Boltzmann's constant:

$$\frac{dw}{dt} = De^{-(E/RT)} \tag{6}$$

W4: Modified Usui wear rate model by adding an exponent on the relative velocity Eq. (4):

$$\frac{dw}{dt} = A'\sigma_n v_{rel}^{0.5} e^{-B/T} \tag{7}$$

W5: Vibration-adjusted Usui's wear rate equation Eq. (4); a constant term is added to the relative velocity to account for vibrations not included in the chip formation model:

$$\frac{dw}{dt} = A''\sigma_n(v_{rel} + 10)e^{-B/T} \tag{8}$$

2.2.1. Wear model constants

Constants for Usui's model (W1) were determined by Lorentzon and Järvstråt [11] by calibrating machining simulations with measured wear rates: First, tool wear machining tests for the selected material were performed; then FE simulations were made under the same conditions; and finally the constants of the wear rate model were calculated by regression analysis, giving the constants $B = 8900$ and $A = 1.82 \times 10^{-12}$. This value of the B parameter is also used here, although the friction coefficient in the chip formation model differs because it is now calibrated with respect to feed force. For this reason, the A parameter was adjusted to give the same crater depth as in the experiments. The same methodology was used to calibrate A, D, A' and A'' for the wear models W1, W2, W3, W4 and W5. The calibrated parameters are presented in Tables 2 and 3. The activation energy in W3 Eq. (6), E, was set to 75.35 kJ/mol [25].

Table 3
Wear model parameters for W1 for the different friction models

	F1 (Coulomb)	F2 (Shear)	F3 (Adjusted)
W1	$A = 1.25 \times 10^{-12}$ $B = 8900$	$A = 1.52 \times 10^{-12}$ $B = 8900$	$A = 1.08 \times 10^{-12}$ $B = 8900$

3. Analysis steps

In a turning operation, a stationary condition with respect to temperature and forces will generally be reached almost immediately after the tool has penetrated the workpiece and subsequently the initial transient of the chip formation has been neglected in predictions of the tool wear progress. Instead, tool wear predictions are made on stationary chip formation conditions, and the first step in tool wear predictions is therefore to calculate the stationary chip condition. Finally, the wear model is activated in the chip formation analysis and the progress of tool wear is calculated.

3.1. Chip formation

In order to reach stationary conditions in FE chip formation simulations using the Lagrangian method, the entire object, on which chip formation simulation is to be performed, must be present and meshed from the beginning of the simulation. Consequentially a transient analysis for reaching steady-state conditions would be computationally prohibitive [26]. Fortunately, by lowering the thermal capacity of the tool, it is possible to reach equilibrium faster; in our case this was obtained after about 1500 increments, see Fig. 5.

The reason for this is that lowering the thermal capacity has the same effect as taking proportionally longer time increments in the thermal calculations compared to the mechanical increment, as can be seen in Eq. (5). Note that the left-hand side vanishes at steady state, while an increased C_p increases the rate of change and correspondingly accelerates, reaching the steady-state condition:

$$\rho C_p \frac{\partial T}{\partial t} = k\left(\frac{\partial^2 T}{\partial x^2} + \frac{\partial^2 T}{\partial y^2} + \frac{\partial^2 T}{\partial z^2}\right) \tag{9}$$

Here, T is the temperature, k is the thermal conductivity, ρ is the density, and C_p is the thermal capacity.

3.2. Tool wear

The tool wear model consists of a FE chip formation model and a wear model implemented as subroutines calculating the wear rate at contact points, modifying the tool geometry accordingly. The wear rate is calculated using Usui's empirical wear model for every node of the tool in contact with the base material. In order

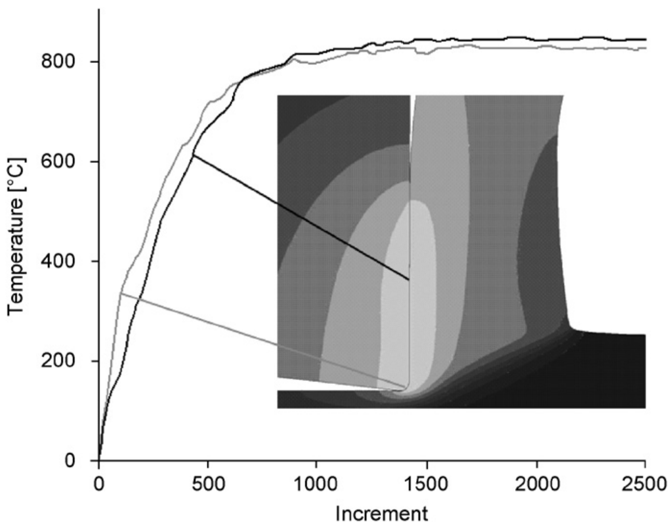

Fig. 5. Temperature history for two nodes in the tool, using thermal capacity acceleration.

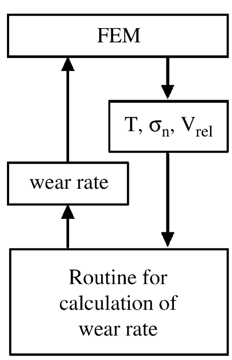

Fig. 6. Schematic illustration of the system for tool wear calculations.

to do this, the temperature, relative velocity, and contact stress are calculated in the FE chip formation simulation for all nodes of the tool in contact with the workpiece. The calculated values are then employed by a user subroutine to calculate the wear rate, see Fig. 6. Based on the calculated wear rate, the geometry of the tool is then updated by moving specific nodes of the tool in the FE chip formation simulation, see [5] for a more comprehensive description. The direction a node is moved is based on the direction of the contact pressure at that node. After moving the node, all integration point data are mapped to the new integration point positions and the chip formation simulation continues, with the tool penetrating through the work material. Updating the geometry distorts the elements of the tool. To avoid this, the tool mesh is automatically remeshed using the "advancing front quad" remeshing technique, at a prescribed frequency.

The wear calculations are started at increment 1800, see Fig. 5, with the tool at steady state with respect to both force and temperature. The wear calculation is subdivided into about 1200 increments, each with tool geometry updating. Using fewer increments would cause convergence problems and numerical errors; using more increments, however, would unnecessarily increase the computation time. The wear calculation corresponds to approximately 15 s of dry machining, resulting in about 65 μm flank wear land and about 5.3 μm deep crater at rake face. Hence, the wear process is accelerated by about 10,000 times in the simulation model.

4. Experiments

Turning experiments were conducted for calibration of friction and wear parameters and for comparison of the simulated and measured wear profiles.

4.1. Experimental conditions

The turning experiments were carried out in a CNC lathe under dry cutting conditions. One cutting speed, vc, 45 m/min and one feed rate, *f*, 0.1 mm/rev were evaluated. The turning length machined during each experiment was 12 mm. The experiment was conducted with 3 replicates. The workpiece was a bar of aged and forged Inconel 718 that was predrilled at its end face to achieve pipe geometry in order to accomplish near orthogonal cutting conditions in the turning operation. The workpiece had a 35.6 mm outer diameter and a 29 mm inner diameter. The tool used for these turning experiments was a triangular, uncoated cemented carbide turning insert with a cutting width of 16 mm. Carbide classification is in accordance with ISO standard N10-N30.

4.2. Measurements

The cutting forces, the chip shape, the cutting edge radius, and the tool wear were all measured in these experiments. The cutting forces (the cutting force, Fc, the feed force, Ff, and the passive force, Fp) were measured for all samples using a three-component dynamometer (Kistler, Type 9121), a multi-channel charge amplifier (Kistler, Type 5017B), and a data acquisition system. The chip shape was investigated for one sample using optical microscopy. For this purpose, the chips produced during each trial were collected, mounted onto specimen holders, grounded and polished. After this, the shape was investigated and the thickness was measured from the obtained images. For calibration and experimental verification, wear profiles for the flank and the rake faces, as well as the cutting-edge radius, were measured for two cutting inserts. These measurements were performed at Toponova AB (www.toponova.se) using white-light interferometry, see e.g. [27] for a description. A schematic illustration of the tool in 3D with a cross-section where the worn and initial tool geometry was measured is presented in Fig. 7.

5. Results

In this section, the impact of the wear and friction model on the simulated wear profile is presented together with measured wear profiles. Simulated temperature, relative velocity and contact pressure are also presented in order to emphasise and clarify the differences between the friction models. Finally, simulated cutting forces and chip thickness are compared with measurements.

5.1. Influence of wear model on wear profile

In this section, the Coulomb friction model (F1) is used and simulated wear profiles are compared with measured profiles using different wear equations.

5.1.1. Crater wear

The simulated crater wear profile using Usui's wear equation (W1) has a maximum crater depth in the upper region of the contact zone on the rake face, at about 200 μm from the start of the rake face. This is in contrast to the measured wear profile having a maximum crater depth close to the tool tip, at only about

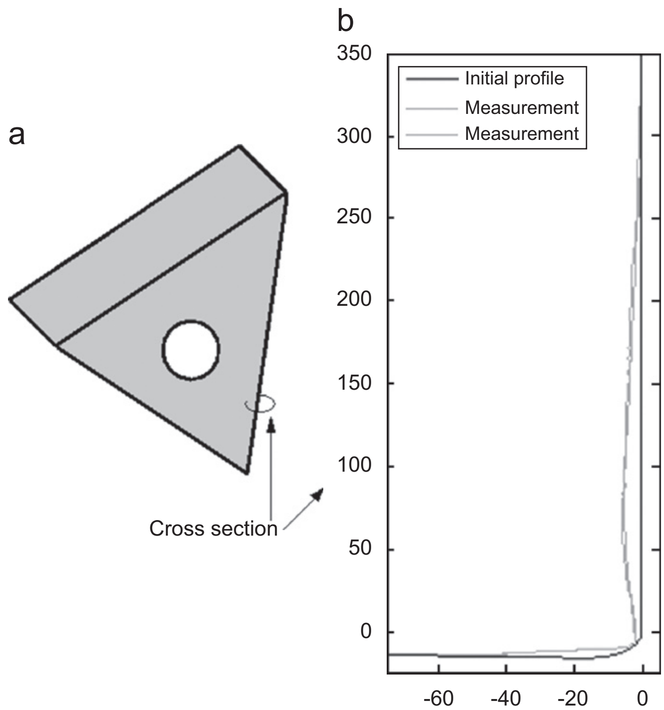

Fig. 7. (a) Schematic illustration showing the 3D tool in and (b) cross section of the worn and initial tool geometry (length scale in μm).

70 μm from the start of the rake face, see Fig. 8. Furthermore, the wear at the tool tip is considerably underestimated.

Reducing parameter B in the wear equation (W2) changes the simulated wear profile slightly, by an even larger underestimation of the amount of wear at the tool tip and moving the position of maximum crater depth somewhat further away from the tool tip.

The simulated wear profile using the vibration-adjusted Usui model (W3) shows better agreement with the measured wear profile in the region just above the tool tip than the original Usui model. However, the position of the maximum crater depth shows only minor changes compared to the original Usui model, and is still located too far away from the tool tip.

The simulated wear profile using the modified Usui with an exponential dependency on the velocity (W4) shows the same tendency as the vibration-adjusted Usui model (W3), but with better agreement with the measured wear profile than the original Usui in the region just above the tool tip. In this case the crater is located somewhat closer to the tool tip. The discrepancy with the measurement is, however, still substantial.

The simulated wear profile using the diffusive model (W5) is radically different, with an almost constant wear rate over the tool–chip interface causing too much wear in the tool tip region. Also in this case, however, the simulated maximum crater depth is positioned too far from the tool tip compared to the measurement.

5.1.2. Flank wear

The simulated flank wear profile using Usui's wear equation (W1) underestimates the wear near the tool tip, see Fig. 8. Lowering the temperature-dependent parameter B in the wear equation (W2) changes the profile at the end of the flank land, while only minor changes can be seen at the beginning of the flank, near the tool tip. Adding a vibration term (W3) gives no significant change in the simulated wear profile. In contrast, the Usui model modified with an exponential dependency (W4) on the velocity provides good agreement with the measured profiles.

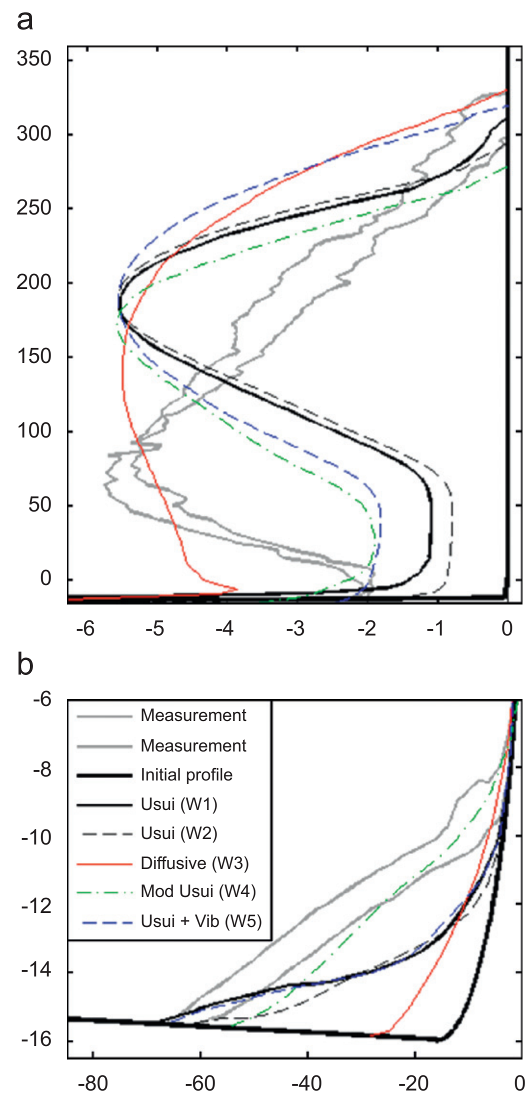

Fig. 8. Simulated wear profiles using different friction models (measured wear profiles and initial tool profile as in Fig. 7; (a) the rake face scaled to emphasise (length scale in μm), (b) the flank face scaled to emphasise (length scale in μm).

The diffusive model (W5) is shown to give a large discrepancy compared to measurement, in particular in flank wear length.

5.2. Influence of friction model on wear profile

In this section the Usui wear equation (W1) is used throughout, and simulated wear profiles are compared with measured profiles using different friction models.

5.2.1. Crater wear

Simulating wear using the Coulomb friction model (F1) predicts a location of the maximum crater too far from the start of the rake face, as stated above. Also, the wear at the tool tip is considerably underestimated compared to the measured wear profile, see Fig. 9.

The same tendency is observed in the simulations using the shear friction model (F2). Indeed, the maximum crater wear in this model is found somewhat further away from the tool tip, while the wear at the tool tip correlates slightly better with the measurements.

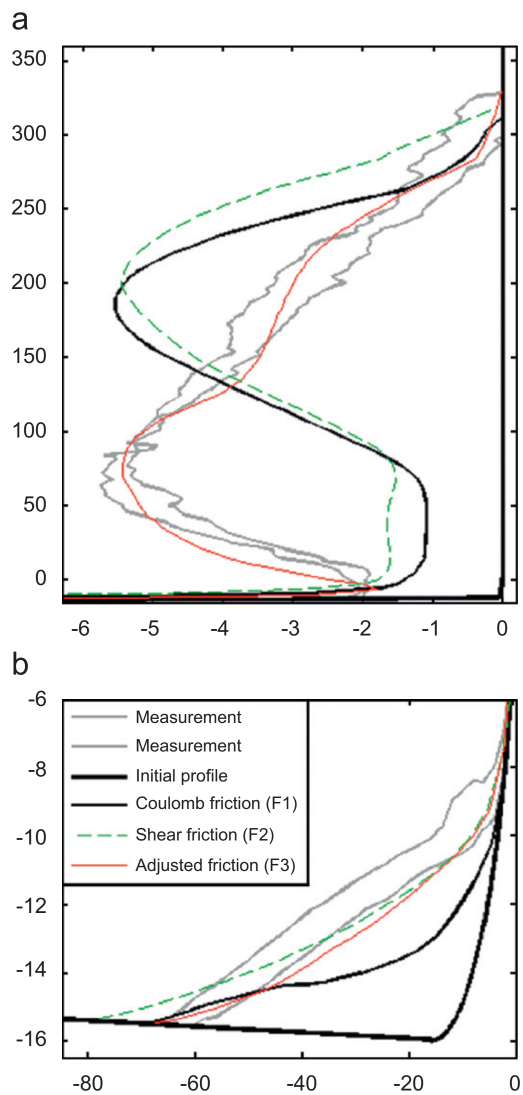

Fig. 9. Simulated wear profiles using different friction models (measured wear profiles and initial tool profile as in Fig. 7); (a) the rake face scaled to emphasise (length scale in μm), (b) the flank face scaled to emphasise (length scale in μm).

The adjusted friction model with a reduced friction coefficient in the area closest to the tool tip (F3), however, predicts a maximum crater depth positioned at the proper location as given by the measurements, while also having the same general shape as the measured profiles. There are still some differences, such as a kink at the position where the friction coefficient is changed. However, the difference between simulations and measurements is of the same magnitude over the entire wear profile as the difference between the two measured wear profiles.

5.2.2. *Flank wear*

Considering the wear at the flank face, the simulation using Coulomb friction (F1) underestimates the amount of wear near the tool tip, see Fig. 9. However, both the shear friction model (F2) and the adjusted friction model with reduced friction coefficient around the tool tip (F3) show good agreement with the measured wear profile at the flank face. Although, the shear friction model predicts too large a flank wear land compared to the measurement, contrary to the adjusted friction model also showing good agreement with respect to length of the flank wear land.

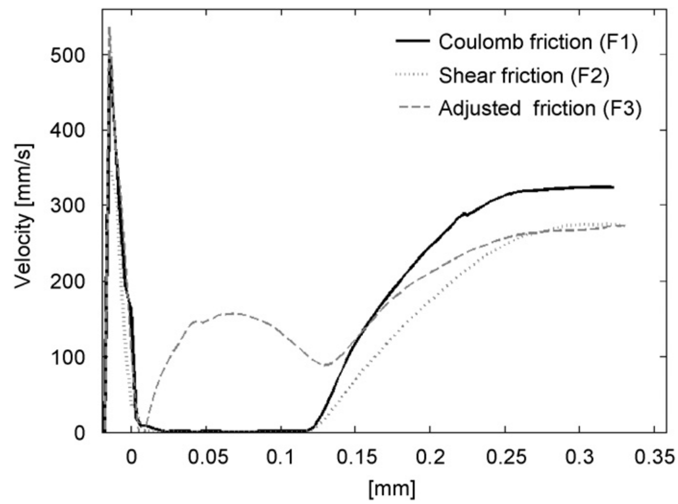

Fig. 10. Velocity profile.

5.3. *Influence of friction on temperature, relative velocity and contact pressure*

In this section, predicted temperature, relative velocity and contact pressure using different friction models are presented for initial tool geometry, for stationary conditions with respect to tool forces and temperature (see Fig. 5), to emphasise and clarify the mechanism through which friction models influence wear rate.

5.3.1. *Relative velocity*

The relative velocity between the tool and the work material can be seen in Fig. 10 for the different friction models. For both the Coulomb model (F1) and the shear friction model (F2) with constant friction coefficients, a region can be observed where the velocity is zero or close to zero. Although the material in this part of the contact zone is stationary relative to the tool, the chip is still moving. The sticking is caused by the internal material friction (plasticity) being lower than the friction between the chip and the tool. The velocity profile will thus be zero at the contact between the tool and the chip, gradually increasing about 40 μm into the chip and then stabilizing; this phenomenon was presented by Desalvo and Shaw [28]. The larger the friction coefficient, the larger this region of stationary, non-moving material and a large friction coefficient is necessary for good correlation between the simulated and measured feed force and contact length. However, by using a reduced friction coefficient around the tool tip, the velocity profile changes dramatically in the "stagnant" region (from 0.01 to 0.14 mm in Fig. 10).

5.3.2. *Temperature*

The impact of friction model on predicted temperature in the tool in contact with the work piece can be seen in Fig. 11. The highest temperature is observed using the Coulomb friction model (F1), while the lowest is observed when using a Coulomb model with reduced friction in the tool tip region (F3). The difference in temperature prediction between the models is less than approximately 40 °C, with the shear model (F2) predicting temperatures in between the two others. The higher predicted temperature with constant Coulomb friction (F1) than the model with reduced friction (F3) may seem counterintuitive, as the heat generated by contact friction is lower. However, the heat generated by plastic deformation is instead correspondingly higher, as the relative motion is accommodated by material deformation, and in addition to this the material remains in this zone for a longer time and consequently transports less of the generated heat away from this zone.

For all models the temperature does not vary by more than about 150 °C over the contact length and the shapes of the temperature profiles are very similar. It is, however, even more interesting that the temperature varies less than 25 °C over about three-quarter of the contact zone, from 0 to about 0.25 mm in Fig. 11, the area where the tool wear is highest, as seen in Fig. 9.

5.3.3. Contact pressure

Fig. 12 shows that the contact stress is highest at the tip of the tool, and that the maximum contact stress is very high, above 2.5 GPa. Furthermore, the contact stress at the rake face stabilizes at two plateaus, one high, close to the tool tip, and one low, further up on the rake face. Interestingly enough, the contact pressure is very similar for all the different friction models, even though the contact lengths differ to some extent.

5.3.4. Cutting forces and chip thickness

In this section, simulated cutting forces, chip thicknesses and contact lengths are presented and compared with measurements, see Table 4. The feed force (F_f) was used to calibrate the chip formation model. The cutting force (F_c), the chip thickness and the contact length were used for validation, showing less than 5% deviation.

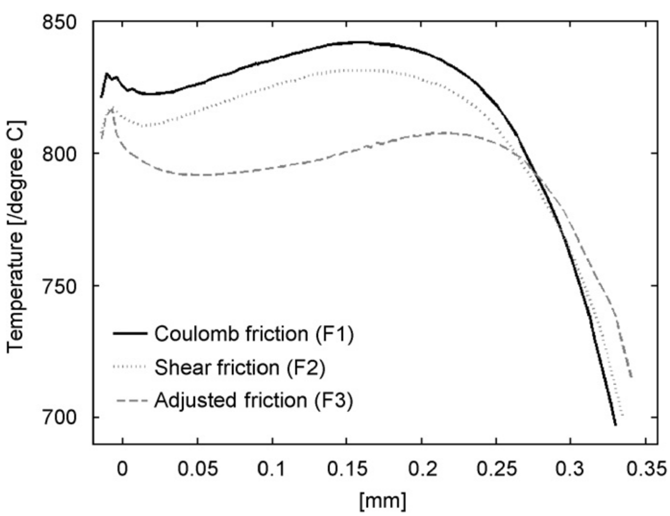

Fig. 11. Temperature profile.

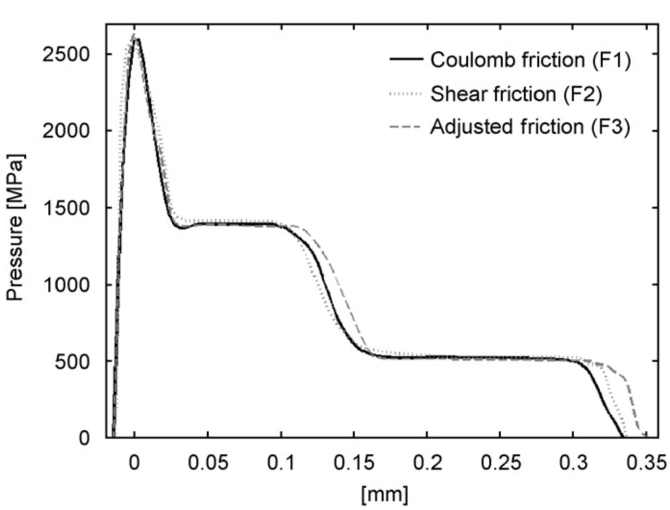

Fig. 12. Pressure along tool–chip interface.

Table 4
Cutting forces, chip thickness and contact lengths

	F_c (N)	F_f (N)	Chip thickness (μm)	Contact length (μm)
Coulomb	1141	774	234	312
Shear	1148	808	237	320
Adjusted	1134	771	231	325
Measured (Standard deviation)	1132 (15.3)	785 (11.8)	228	314±14

6. Discussion

It can be seen that quantitative agreement with measured wear is not possible using Coulomb friction (F1), regardless of which wear model is used. The largest discrepancy when using Usui's wear model (W1) is found in the region around the tool tip, between 0 and 100 μm in Fig. 8. The simulated wear profile can be changed somewhat by employing other wear models, but it seems impossible to achieve a correct position of the maximum crater depth, as shown by simulations employing wear models similar to the Usui model (W2, W4 and W5). This can be understood by studying the relative velocity graph (Fig. 10). This graph shows that simulations with traditional, constant coefficient, friction models (F1 and F2) predict zero velocity in the region where the highest measured crater depth is found. It would not help to vary pressure or temperature either, as Figs. 11 and 12 show them to be very constant over the area of the wear peak—the temperature varies less than 25 °C. Thus, it is still too high up on the flank, and the shape of the crater is quite different from those measured. Applying a diffusion wear model (W3) which completely disregards the effect of velocity does allow a slightly better prediction of the position of maximum crater depth, but still too high, and the crater shape is very different from the measured ones.

Having argued that it is insufficient to improve the wear model for quantitative and qualitative prediction of the wear profile, instead, it is necessary to improve the simulation accuracy in the variables affecting wear. Of the three local variables in the wear model, the temperature and pressure distributions along the rake face seem impossible to influence enough to provide the observed wear shape through realistic model changes. The relative velocity, however, is dramatically influenced by friction. It seems reasonable to assume that the validity of Coulomb friction breaks down as the material approaches its yield limit. A very good agreement with the measured wear profiles was subsequently achieved by adding the reasonable physical assumption that the friction coefficient is lower in the vicinity of the tool tip where the contact pressure is extremely high (F3). Note that the excellent experimental agreement in chip formation (cf. Table 4) is retained. Obviously, our friction "model" F3 with a change in friction parameter over a specified region is rather arbitrary, and should be replaced by an improved theoretically and experimentally founded model with similar characteristics, i.e. a cap on friction stress at high contact pressures.

7. Conclusion

A finite element tool wear model that can predict the worn geometry quantitatively in cemented carbide tool machining nickel-based alloys has been developed. To achieve this, different wear and friction models have been investigated with respect to their impact on parameters affecting the wear process, such as temperature and relative velocity. A strong conclusion from this is that the friction model has a major influence on the simulated wear profile, by influencing the relative velocity. The proposed friction description with a lower coefficient in the area around the tool tip together with Usui's empirical wear equation shows excellent experimental agreement. Thus, it would be of great interest to direct experimental and theoretical efforts at investigating high contact pressure friction for achieving a more realistic friction model for machining than the Coulomb friction model commonly employed.

Acknowledgements

This study was supported by NFSM (The National Graduate School in Material Science), MERA (Manufacturing Engineering Research Area) and the Volvo Aero Corporation.

References

[1] P.K. Wrigth, J.G. Chow, Deformation characteristic of nickel alloys during machining, Journal of Engineering Materials and Technology 104 (2) (1982) 85–93.
[2] A.V. Tipnis, Influence of metallurgy on machinability, American Society for Metals 7 (1975).
[3] M.C. Shaw, Metal Cutting Principal, Clarendon, Oxford, 1997.
[4] T. MacGinley, J. Monaghan, Modelling the orthogonal machining process using coated cemented carbide cutting tools, Journal of Materials Processing Technology 118 (2001) 293–300.
[5] Y.-C. Yen, J. Anurag, T. Altan, A finite element analysis of orthogonal machining of different tool edge geometries, Journal of Materials Processing Technology 146 (2004) 72–81.
[6] T. Altan, F. Koppka, P. Sartkulvanich, Determination of flow stress for metal cutting simulation—a progress report, Journal of Materials Processing Technology 146 (1) (2004) 61–71.
[7] C. Hortig, B. Svendsen, Simulation of chip formation during high-speed cutting, Journal of Materials Processing Technology 186 (2007) 66–76.
[8] Y.-C. Yen, J. Söhner, B. Lilly, T. Altan, Estimation of tool wear in orthogonal cutting using the finite element analysis, Journal of Materials Processing Technology 146 (2004) 82–91.
[9] L. Filice, F. Micari, L. Settineri, D. Umbrello, Wear modelling in mild steel orthogonal cutting when using uncoated carbide tools, Wear 262 (2007) 545–554.
[10] L.-J. Xie, J. Schmidt, C. Schmidt, F. Biesinger, 2D FEM estimation of tool wear in turning operation, Journal of Materials Processing Technology 258 (2005) 1479–1490.
[11] J. Lorentzon, N. Järvstråt, Tool Wear Geometry Updating in Inconel 718 Turning Simulations, in: 9th CIRP International Workshop on Modeling of Machining Operations, May 11–12, 2006, pp. 491–498.
[12] T.H.C. Childs, Friction modelling in metal cutting, Wear 260 (2006) 310–318.
[13] T. Özel, The influence of friction models on finite element simulations of machining, International Journal of Machine Tools & Manufacture 46 (2006) 518–530.
[14] E. Usui, T. Shirakhashi, T. Kitagawa, Part 3: Analytical prediction of three dimensional cutting process, Transactions of ASME, Journal of Engineering for Industry 1 (1978) 33–38.
[15] T. Kitagawa, K. Maekawa, T. Shirakhashi, E. Usui, Analytical prediction of flank wear of carbide tools in turning plain carbon steels (Part 1), Bulletin of the Japan Society of Precision Engineering 22 (4) (1988) 263–269.
[16] T. Kitagawa, K. Maekawa, T. Shirakhashi, E. Usui, Analytical prediction of flank wear of carbide tools in turning plain carbon steels (Part 2), Bulletin of the Japan Society of Precision Engineering 23 (2) (1989) 126–134.
[17] H. Takeyama, R. Murata, Basic investigation of tool wear, Journal of Engineering for Industry (1963).
[18] N. Ahmed, A.V. Mitrofanov, V.I. Babitsky, V.V. Silberschmidt, Analysis of material response to ultrasonic vibration in turning Inconel 718, International Journal of Materials Science and Engineering A 424 (2006) 318–325.
[19] N. Fang, A quantitative sensitivity analysis of the flow stress of 18 engineering materials in machining, Proceedings of the ASME Manufacturing Engineering Division 14 (2003) 23–32.
[20] R. Sievert, A.-H. Hamann, D. Noack, P. Löwe, K.N. Singh, G. Künecke, Simulation of thermal softening, damage and chip segmentation in a nickel super-alloy, in: H.K. Tönshoff, F. Hollmann (Eds.), Hochgeschwindigkeitspannen, Wiley, New York, 2005, pp. 446–469.
[21] W.J. Zhang, B.V. Reddy, S.C. Deevi, Physical properties of TiAl-base alloys, Scripta Materialia 45 (2001) 645–651.
[22] E.M. Trent, Metal Cutting, Butterworth, London, 2000 Isbn:0-7506-7069.
[23] N.N. Zorev, Interrelationship between shear processes occurring along tool face and on shear plan in Metal Cutting, in: Proceedings of the International Research in Production Engineering Conference, ASME, New York, 1963, pp. 42–49.
[24] L. Filice, D. Umbrello, F. Micari, L. Setteneri, On the finite element simulation of thermal phenomena in machining process, in: Keynote Eighth International ESAFORM Conference, April 27–29, Cluj-Napoca, Romania, 2005, pp. 729–732.
[25] Diffusion and Defect Data, 27, Trans Tech Publications, Rockport, MA, 1982.
[26] F. Klocke, H.-W. Raedt, S. Hoppe, 2D-FEM simulation of the orthogonal high speed cutting process, Machining Science and Technology 5 (3) (2001).
[27] A. Devillez, S. Lesko, W. Mozer, Cutting tool crater wear measurement with white light interferometry, Wear 256 (2004) 56–65.
[28] G.J. DeSalvo, M.C. Shaw, Hydrodynamic action at a chip–tool interface, in: Proceedings of the ninth International MTDR Conference, Birmingham, 1968, pp. 961–971.